ACS Catalysis

pubs.acs.org/acscatalysis

Research Article

Discovery of Semi-Pinacolases from the Epoxide Hydrolase Family during Efficient Assembly of a Fungal Polyketide

Fei Cao, Wen-Tao Tao, Qian Yu, Chu-Xuan Xu, Jin-Tao Cheng, Ruo-Xi Liu, Qing-Wei Zhao, Xin-Hang Jiang, Yu Liu, Yong-Quan Li, Zha-Jun Zhan,* Ting Shi,* and Xu-Ming Mao*

Cite This: *ACS Catal.* 2021, 11, 14702−14711

Read Online

ACCESS | Metrics & More | Article Recommendations | Supporting Information

ABSTRACT: The semipinacol rearrangement (SPR) is highly useful in the asymmetric synthesis of complex compounds. In biological systems, only a few semi-pinacolases belonging to a few families have been identified to catalyze the SPR on alkaloids. Here, based on the biosynthesis of a fungal mycotoxin asteltoxin (**1**), two semi-pinacolases AstD/MrvD were identified from the epoxide hydrolase family to catalyze type III SPR on the polyketide backbone. They were proposed to catalyze efficient regio-selective hydrolysis on the bis-epoxide and 2,3-migration on the epoxide alcohol for the rearrangement. Based on the comprehensive mutations and chemical calculations, a critical Asp residue was identified as an acid for the coupled catalysis of selective epoxide collapse and subsequent SPR, while other critical residues facilitated efficient hydrolysis and protected carbocation for SPR. Thus, this study expanded the SPR biocatalyst family and provided an understanding of the catalytic mechanisms of these bifunctional semi-pinacolases.

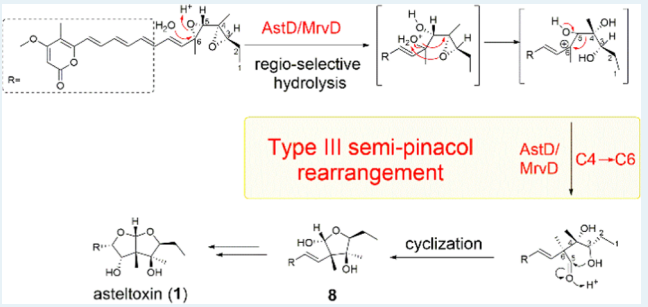

KEYWORDS: *semipinacol rearrangement, epoxide hydrolase, catalysis, natural product, biosynthesis*

INTRODUCTION

The semipinacol rearrangement (SPR) is highly reliable for the efficient asymmetric synthesis of complex compounds.[1,2] During the reactions, the vicinal nucleophilic migrating groups often attack the oxirane carbons in high regio- and stereo-selectivity, usually *anti* to the epoxide, leading to a quaternary carbon center.[3,4] Depending on the electrophilic carbon center, four types of SPR (Scheme 1a) have been proposed and strategically utilized,[4] and type III SPR mainly focuses on derivatives of 2,3-epoxy alcohol as the substrates with various migrations for product diversity.[5−7]

Semi-pinacolases (SPases) are the biocatalysts for this fantastic rearrangement to develop the structural complexity of natural products. To date, several SPases have been identified in limited families only with alkaloids as the substrates (Scheme 1a). Most SPases are bifunctional enzymes belonging to flavin-dependent monooxygenases (FMOs) (NotI/NotI′, NotB, PhqK, FqzB, AuaG, CtdE)[8−14] and the P450 monooxygenase (CyaH)[15] to catalyze epoxidation on indole/quinolone alkaloids to produce epoxy amines and subsequent SPR. Other SPases include the NTF2-like superfamily enzyme (BvnE)[16] and a bifunctional cytochrome P450 (FtmG)[13] to catalyze SPR after hydroxylation on the indole of alkaloids. Meanwhile, most of these SPases catalyze the migration of substituent groups (mostly prenyl groups) (Schemes 1a and S1−S3).

Given the intriguing roles and scarcity of SPases, our seeking of novel SPases was inspired by the proposed biosynthesis of a fungal mycotoxin asteltoxin (**1**).[17,18] **1** is a natural polyketide with an intriguing 2,8-dioxabicyclo-[3.3.0]-octane ring (or bis-tetrahydrofuran, bis-THF),[19] which is essential for the toxicity of **1** as an inhibitor of the mitochondrial adenosine 5′-triphosphate (ATP) synthase.[20] This moiety has been supposed to be derived from multiple epoxidations on the terminal polyene, subsequent 3,4-epoxide hydrolysis to afford an epoxy alcohol, and 2,3-migration for the rearrangement of the polyketide backbone, followed by the formation of a hemiacetal intermediate[17,18,21] (Scheme 1b, route b). This proposed rearrangement is type III SPR on the polyketide backbone in a C1 → C3 migration manner, clearly distinct from the SPR catalyzed by reported SPases (type II, type III in R3 → C3 migration, and type IV) (Scheme 1a and S1−S3). This proposed involvement of SPR for **1** biosynthesis implied a unique SPase in this biosynthetic pathway.

1 is structurally related to fungal mycotoxins aurovertins (**2**−**4**) from *Calcarisporium arbuscula*[22,23] and citreoviridin from

Received: August 27, 2021
Revised: November 14, 2021
Published: November 23, 2021

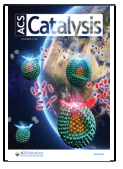

https://doi.org/10.1021/acscatal.1c03899
ACS Catal. 2021, 11, 14702−14711

Scheme 1. Proposed Semipinacol Rearrangement for Asteltoxin (1) Biosynthesis[a]

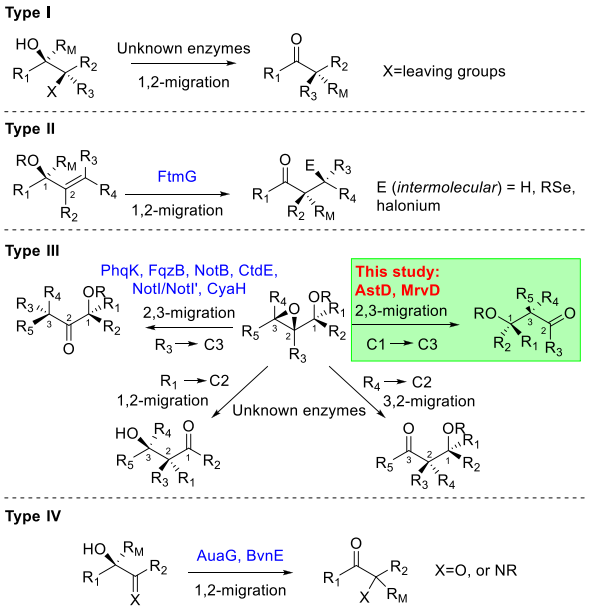

Enzyme	Functional classification	Substrate type	Rearrangement type
FtmG	Cytochrome P450	Indole alkaloid	Type II
FqzB	Flavin-dependent monooxygenase	Indole alkaloid	Type III, R_3→C3
NotB	Flavin-dependent monooxygenase	Indole alkaloid	Type III, R_3→C3
NotI/NotI'	Flavin-dependent monooxygenase	Indole alkaloid	Type III, R_3→C3
PhqK	Flavin-dependent monooxygenase	Indole alkaloid	Type III, R_3→C3
CtdE	Flavin-dependent monooxygenase	Indole alkaloid	Type III, R_3→C3
CyaH	P450 monooxygenase	Indole alkaloid	Type III, R_3→C3
AstD	Epoxide hydrolase	Polyketide	Type III, C1→C3
MrvD	Epoxide hydrolase	Polyketide	Type III, C1→C3
AuaG	Flavin-dependent monooxygenase	Quinolone alkaloid	Type IV
BvnE	NTF2-like superfamily enzyme	Indole alkaloid	Type IV

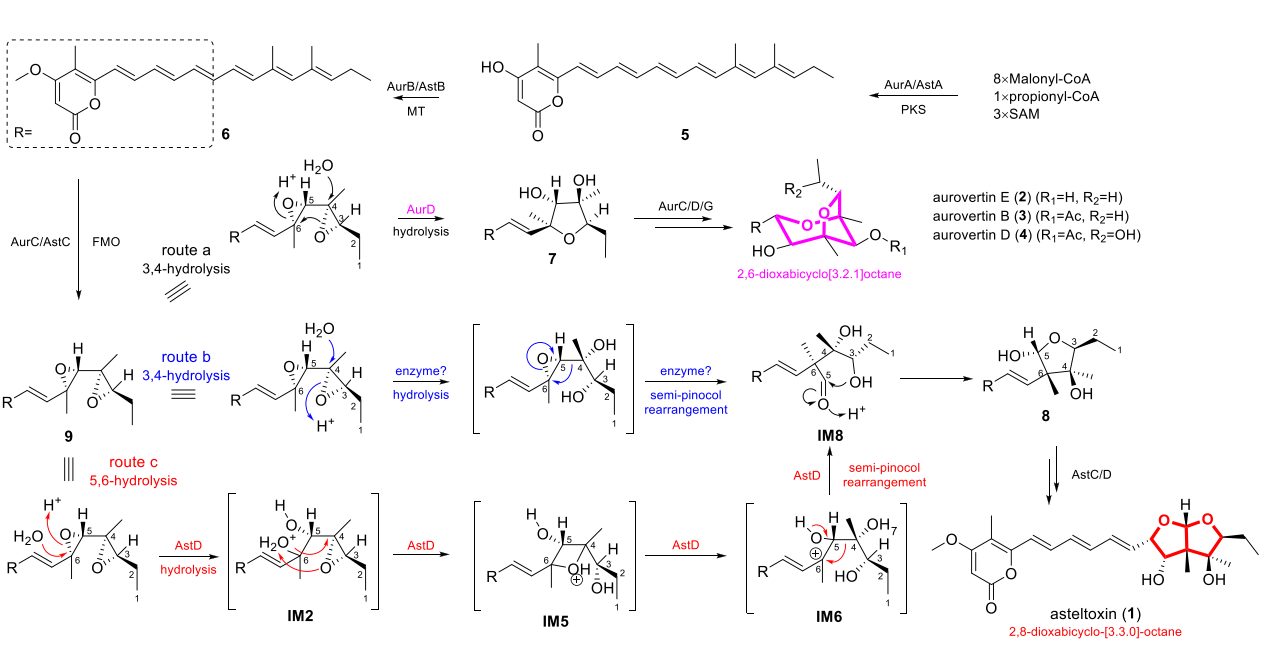

[a](a) Four types of semipinacol rearrangement. The known semi-pinacolases were reclassified, and detailed information is shown in the table on the right panel. (b) Proposed biosynthetic pathways for asteltoxin (**1**) (route b/c) compared with aurovertins (**2**–**4**) (route a) with the same precursors but different hydrolases. 3,4-Epoxide hydrolysis was previously proposed for aurovertins and asteltoxin biosynthesis (route a and b), while 5,6-epoxide hydrolysis was proposed in this work (route c).

Aspergillus terreus[24,25] (Schemes 1b and S4). The 2,6-dioxabicyclo-[3.2.1]-octane ring contained in **2**–**4** has been proposed to be derived from α-pyrone-polyene precursors **5** and **6** through efficient regio-/stereo-selective epoxidations and hydrolysis, exerted by four enzymes including a highly reduced polyketide synthase (PKS) AurA, a methyltransferase (MT) AurB, a flavin-dependent monooxygenase (FMO) AurC, and an epoxide hydrolase (EH) AurD. Both the aurovertin biosynthetic intermediate **7** and citreoviridin contained a tetrahydrofuran (THF) moiety with the same stereochemistry. Biosynthesis of citreoviridin has also been disclosed in the same logic as **7** (Scheme S4). Although no SPR was observed in the biosynthesis of **2**–**4** and citreoviridin, their studies would be helpful to elucidate the biosynthesis of **1** and therefore the underlying SPase.

Here, from the biosynthetic pathway of **1**, two novel bifunctional SPases AstD/MrvD belonging to the epoxide hydrolase (EH) family were identified with a distinct substrate and migration type from the previously reported SPases, and their catalytic mechanisms were also investigated.

RESULTS

Identification of the *ast* Gene Cluster for Biosynthesis of 1. To find this SPase, the *ast* gene cluster responsible

https://doi.org/10.1021/acscatal.1c03899
ACS Catal. 2021, 11, 14702−14711

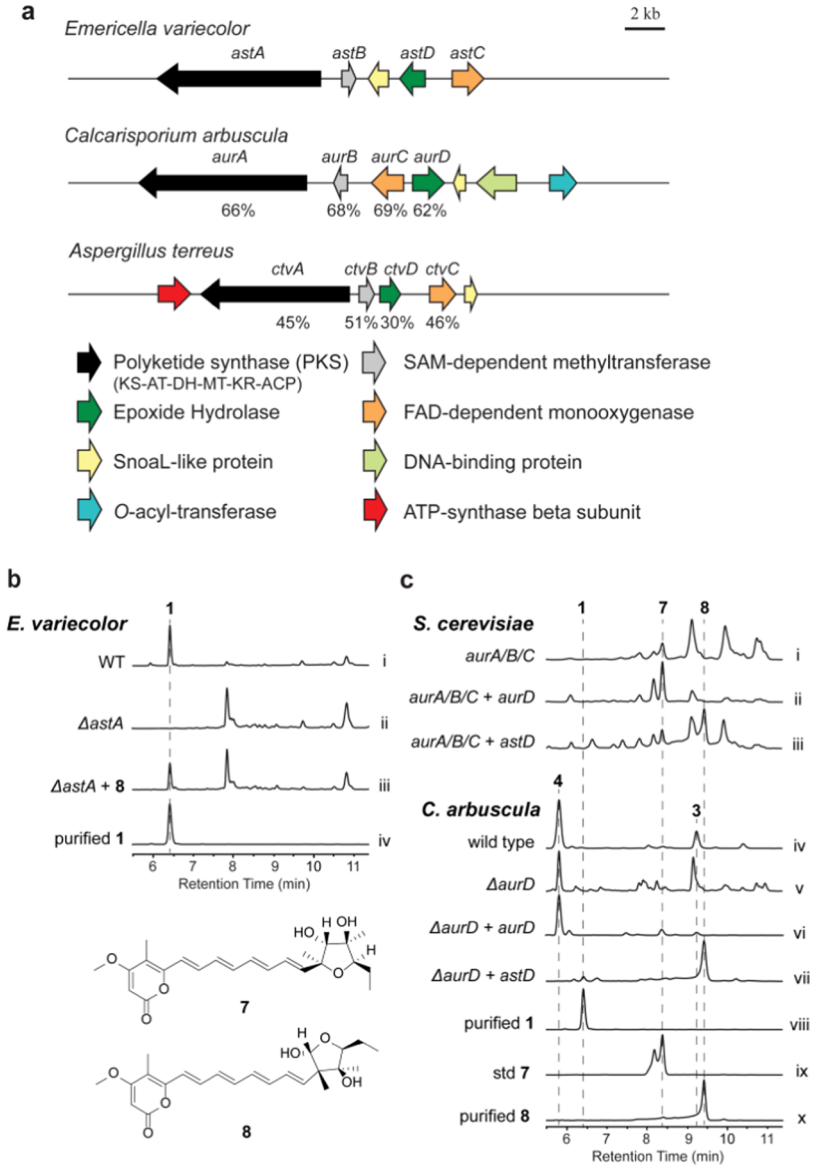

Figure 1. Epoxide hydrolase AstD catalyzes the semipinacol rearrangement for **1** biosynthesis. (a) Gene clusters of asteltoxin from *E. variecolor* and aurovertins from *C. arbuscula*. Protein identity is shown below the *ast* cluster. (b) High-performance liquid chromatography (HPLC) analysis of extracts from *E. variecolor* wild type, Δ*astA* mutant, and Δ*astA* mutant fed with purified **8**. Purified **1** is shown as the standard. (c) HPLC traces of extracts from *Saccharomyces cerevisiae* introduced with *aurABC* and coexpressing *aurD* or *astD*, as well as *C. arbuscula* wild type, Δ*aurD* mutant, and Δ*aurD* mutant complemented with *aurD* or *astD*. Standard **7** and purified **8** are shown as standards.

for **1** biosynthesis was first identified by local BLAST[26] with queries of *aurA-aurD* nucleotide sequences on the genome sequence of a fungal producer of **1** (Figures S1−S3 and Table S7), *Emericella variecolor* NHL 2881.[18] It contained four core genes encoding a PKS AstA, an MT AstB, an FMO AstC, and an EH AstD, which were highly similar to AurA-AurD for aurovertin **2**−**4** biosynthesis[17,18,22] and CtvA-CtvD for citreoviridin biosynthesis,[24] respectively (Figure 1a).

Next, *astA-astD* were individually deleted in *E. variecolor*, and all mutants showed very similar metabolic profiles with the corresponding *C. arbuscula* Δ*aurA*-Δ*aurD* mutants, respectively (Figures S4−S11). Production of **1** was completely abolished in the Δ*astA* mutant (Figure 1b,i−ii), while the Δ*astB* and Δ*astC* mutants predominantly produced α-pyrone-polyenes **5** and **6** as *C. arbuscula* Δ*aurB* and Δ*aurC* mutants, respectively, consistent with the hypothesis that **1** and **2**−**4** were derived from the same precursors **5** and **6** (Scheme 1b). Meanwhile, the Δ*astD* mutant accumulated a series of compounds with the same molecular weight of 402 ($[M + H]^+$ = 403) as the *C. arbuscula* Δ*aurD* mutant, including the aurovertin biosynthetic intermediate **7**. The EH AurD has been proposed to work on the bis-epoxide **9** to produce the intermediate **7** and finally **2** in high regio- and stereo-selectivity (Scheme 1b).[22] However, **9** was supposedly unstable, and spontaneous hydrolysis of **9** in the Δ*aurD* mutant resulted in the production of isomers ($[M + H]^+$ = 403) with a THF moiety[22] (Figure S11).

All above data suggested that this *ast* gene cluster accounted for **1** biosynthesis in *E. variecolor*.

Semipinacol Rearrangement Catalyzed by Epoxide Hydrolase Family Enzymes. With the identification of the *ast* gene cluster, heterologous reconstitution of biosynthetic pathways was further performed in *S. cerevisiae* BJ5464-NpgA[27] to probe the unique SPase referred to previous studies.[24,28−31]

https://doi.org/10.1021/acscatal.1c03899
ACS Catal. 2021, 11, 14702−14711

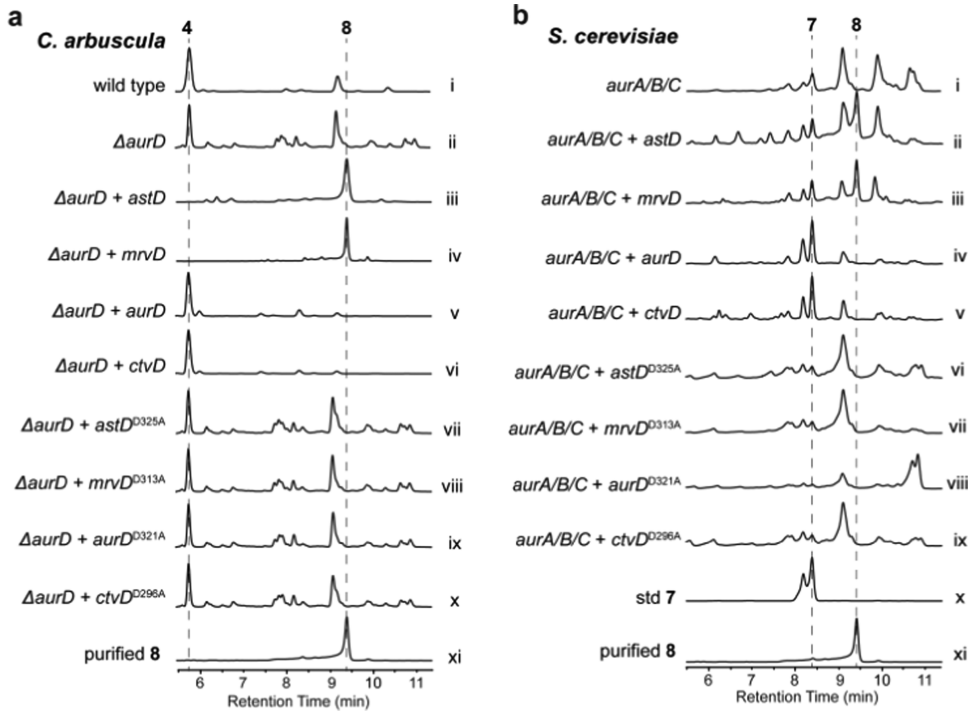

Figure 2. Asp is a critical residue as a general acid for hydrolysis and semipinacol rearrangement. (a) HPLC profiles of extracts from *C. arbuscula* wild type, the Δ*aurD* mutant, and the mutant complemented with *astD*/*mrvD*/*aurD*/*ctvD* and $astD^{D325A}$/$mrvD^{D313A}$/$aurD^{D321A}$/$ctvD^{D296A}$ mutants. Purified **8** is shown as the standard. (b) HPLC traces of extracts from *S. cerevisiae* with *aurA/B/C* and coexpressing *astD*/*mrvD*/*aurD*/*ctvD* and $astD^{D325A}$/$mrvD^{D313A}$/$aurD^{D321A}$/$ctvD^{D296A}$ mutants. Standard **7** and purified **8** are shown for standards.

Combinatory heterologous expression of *astA*, *astA/B*, and *astA/B/C* in yeast produced the same metabolites as an expression of *aurA*, *aurA/B*, and *aurA/B/C*, respectively (Figure S12), suggesting that neither AstB nor AstC was the SPase. However, when *astD* was additionally expressed in *S. cerevisiae aurA/B/C*, a new product **8** ($[M + H]^+$ = 403) was clearly produced with minor production of **7** (Figure 1c,iii). But no **8** was produced if *aurD* was additionally expressed in *S. cerevisiae aurA/B/C*, and **7** was still the main product as reported previously[22] (Figure 1c,ii). To further confirm the AstD-catalyzed production of **8**, *astD* was ectopically expressed in the *C. arbuscula* Δ*aurD* mutant, and **8** was predominantly produced, along with a small amount of **1**, but no production of aurovertins was observed (Figure 1c,vii). However, complementation of *aurD* in the Δ*aurD* mutant restored the full production of aurovertin D (**4**), and no **1** or **8** was produced (Figure 1c,vi).

Our above distinct metabolic profiles from the heterologous biosynthetic pathway reconstitution suggested that EH AstD would be responsible for SPR in the production of **1**. Therefore, this new compound **8** was purified from the *C. arbuscula* Δ*aurD* + *astD* strain, and its structure was elucidated as a new tetrahydrofuranyl pyrone-polyene compound by MS and NMR spectroscopy (Figures S13−S21 and Table S8). As expected, **8** contained a hemiacetal structure, which was supposed to develop from the SPR to form an aldehyde group (Scheme 1b). Importantly, subsequent feeding of **8** into the *E. variecolor* Δ*astA* mutant led to the production of **1** (Figure 1b,iii), confirming that **8** was the authentic on-pathway intermediate for **1** biosynthesis. These data suggested that the EH AstD should be the SPase for the production of the hemiacetal intermediate **8**.

To further exclude the possibility that **8** was produced nonenzymatically or from other enzymes, the LC-MS data from two EH mutants Δ*aurD* and Δ*astD*, as well as yeast cells expressing *aurA/B/C* or *astA/B/C* were carefully checked. All of these strains produced a series of compounds with a molecular weight of 402 ($[M + H]^+$ = 403), including **7**, but not **8** (Figure S22 ii, iv, vi, and vii). These compounds have been supposed from the nonenzymatic hydrolysis of the bis-epoxide **9** at C3−C6 (Scheme 1b, route a), and one of the isomers of **7** has been purified previously with the same planar structure but a subtle stereochemistry difference on THF.[22] The absence of **8** in these strains indicated that no SPR occurred, even though the putative substrate for SPR was supposed to exist after the spontaneous hydrolysis, supporting the necessity of AstD and that the SPR occurred enzymatically *in vivo*. In addition, the SPR product **8** was produced only when AstD was present in fungi (Figure S22 i, v, and viii). These data from three independent fungal genera further supported that it was AstD that catalyzed SPR.

Next, BLASTp was performed with a query of the deduced amino acid sequence of AstD for more potential SPases. Two EHs (accession number: KFG86079.1 and XP_007824469.1) from *Metarhizium anisopliae* E6 and *Metarhizium robertsii* ARSEF 23, respectively, showed the highest identity (both 66%), and their corresponding genes situated in the gene clusters were highly homologous to the *aur* gene cluster (Figure S23). In addition, CtvD has been shown as an EH for citreoviridin biosynthesis in *A. terreus* (Figure 1a and Scheme S4b).[24] Thus, cDNAs of XP_007824469.1 from *M. robertsii* ARSEF 23 (named *mrvD*) and *ctvD* were expressed in the *C. arbuscula* Δ*aurD* mutant and *S. cerevisiae aurA/B/C*, respectively. Interestingly, MrvD remarkably promoted the production of **8** as AstD, both in yeast and *C. arbuscula*

https://doi.org/10.1021/acscatal.1c03899
ACS Catal. 2021, 11, 14702−14711

(Figures 2a,iii–iv and 3b,ii-iii), while no **8** was produced in the cells coexpressing CtvD, just as AurD (Figures 2a,v-vi and

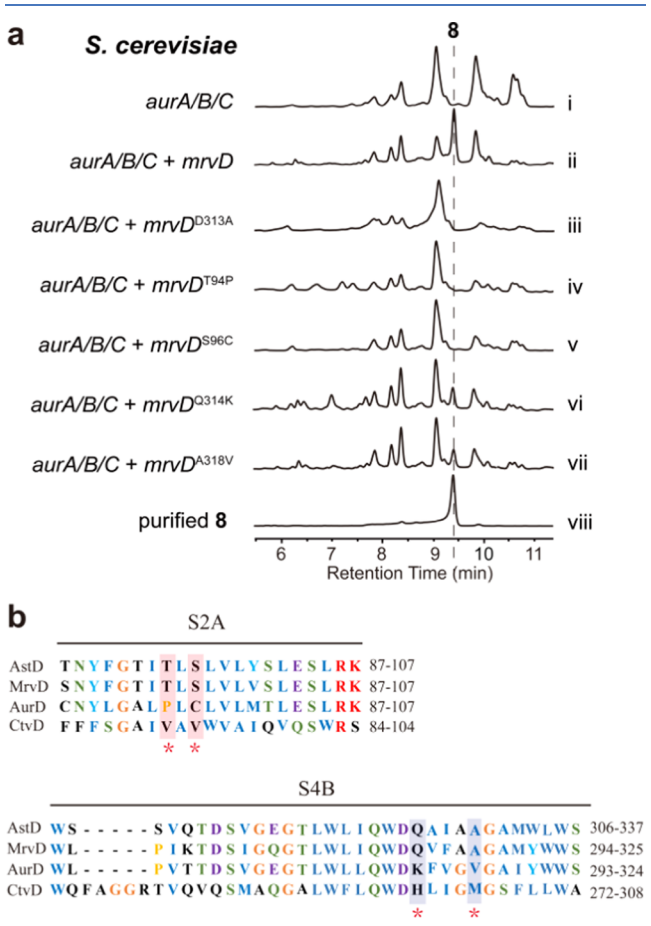

Figure 3. Critical residues for efficient hydrolysis and semipinacol rearrangement. (a) HPLC traces of extracts from *S. cerevisiae* with *aurA/B/C* and coexpressing *mrvD* and *mrvD* mutants. Purified **8** is shown as the standard. (b) Protein sequence alignment of S2A and S4B motifs of EHs. The identified critical residues are labeled with asterisks.

3b,iv-v). These data suggested that the MrvD also catalyzed the SPR, consistent with the observation that **1** could be produced in *M. anisopliae* and *M. robertsii* (Figure S24), while CtvD solely possessed the hydrolase activity as AurD.

Critical Asp Residue for Hydrolysis and Rearrangement. Here, two EHs AstD/MrvD were identified as the SPases. Generally, EHs employ an acidic residue as the general acid[32]/base[33] for epoxide collapse during hydrolysis. For the enzyme-catalyzed SPR and a similar Meinwald rearrangement, particularly with epoxides as the substrates, a general acid is commonly required to protonate the epoxide oxygen for efficient C–O cleavage,[34] as exemplified by E222 in a hydratase PenF and R192 in the FMO PhqK for the catalysis of rearrangement during penigequinolone and paraherquamide biosynthesis,[9,34] respectively. Thus, site-direct mutagenesis was performed to investigate the critical acidic residues for the catalytic activities of these newly identified SPases.

Protein sequence alignment among four EHs showed that nine acidic Asp/Glu residues were highly conserved (Figure S25). When these acidic residues were individually mutated to Ala in AstD, only the AstD^{D325A} mutant completely lost both catalytic activities to produce **8**, either in *C. arbuscula* or in *S. cerevisiae* (Figure 2a,vii and b,vi), while mutations of other acidic residues wholly or partially retained both catalytic activities to produce **8** (Figure S26). Meanwhile, mutation of the corresponding Asp residue (D313) in MrvD also completely abolished **8** production in *C. arbuscula* and *S. cerevisiae* (Figure 2a,viii and b,vii). Mutation of the corresponding Asp residue in AurD or CtvD could neither rescue the chemo-type of the *C. arbuscula* Δ*aurD* mutant (Figure 2a,ix,x) nor confer high production of **7** in yeast (Figure 2b,viii,ix) as their wild-type enzymes. All of these results indicated that this Asp residue in EHs was critically involved in both proper hydrolysis and SPR, and D325/D313 in AstD/MrvD should serve as the general acids for both hydrolysis and SPR.

Other Critical Residues for Efficient Hydrolysis and SPR. Although critical Asp residues for both hydrolysis and SPR have been identified, they were highly conserved in all four EHs, suggesting that there should be other residues/regions in AstD/MrvD specifically accounting for the SPR. For efficient SPR, a favorable microenvironment, such as hydrogen bonds between enzyme-intermediate and the hydrophobic α/β-barrel fold within the enzymes, should be essentially built up to stabilize and protect the carbocation intermediates.[9,16] So, protein shuffling was demonstrated between EHs for these additional critical residues/regions.

Here, MrvD-AurD were chosen as they possessed a higher sequence identity (67%) than AstD-AurD (63%). MrvD-AurD were divided into five regions (S1–S5) for shuffling based on membrane-spanned domains predicted from the TMHMM server (Figures S27 and S28). Biosynthetic pathway reconstitution in *S. cerevisiae* showed that individual substitution of MrvD S2–S4 motifs from AurD severely reduced **8** production (Figure S29). Furthermore, S2A motif substitution completely abolished the production of **8** (Figure S30, iii), and then the critical residues were further narrowed down to T94 and S96. Individual mutation of two residues in MrvD to Pro and Cys as in AurD (Figure 3b), respectively, abolished production of **8** completely in yeast and conferred a very similar metabolite profile with *S. cerevisiae aurA/B/C* and *aurA/B/C* + *mrvD*^{D313A} (Figure 3a,i–v). These data suggested that both residues in MrvD were essential for proper catalysis of both hydrolysis and subsequent SPR.

Further substitution of MrvD S2B, S3A, and S4B motifs with the corresponding fragments from AurD also severely reduced **8** production (Figures S30–S32). Additional mutations of the 14 different residues from these three motifs of MrvD showed that Q314K or A318V mutation (Figure 3b) severely reduced **8** production (Figure 3a,vi–vii), along with a moderate reduction of **8** production from four MrvD mutants (G127A in S2B, A201T in S3A, A317G and M321I in S4B) (Figures S30–S32). We thus suspected that the side chains of these key residues might form a favorable microenvironment to ensure efficient SPR cooperatively. Moreover, these key residues identified above were highly conserved in MrvD/AstD but not in AurD/CtvD (Figures S30–S32), suggesting that MrvD/AstD shared the same mechanism for catalysis.

Nevertheless, when a mutant AurDm was created after all 19 different residues in S2, S3A, and S4B of AurD were altered to the corresponding residues in MrvD, this mutant still conferred a similar metabolite profile as AurD, and no **8** production was observed (Figure S33). These data suggested that there was an additional catalytic mechanism for SPR, which the above-identified critical residues could not fully account for.

https://doi.org/10.1021/acscatal.1c03899
ACS Catal. 2021, 11, 14702–14711

Scheme 2. DFT Calculations of Proposed Models of Reaction Pathways for the Biosynthesis of Compound 8 or 7 with/without the Semipinacol Rearrangement[a]

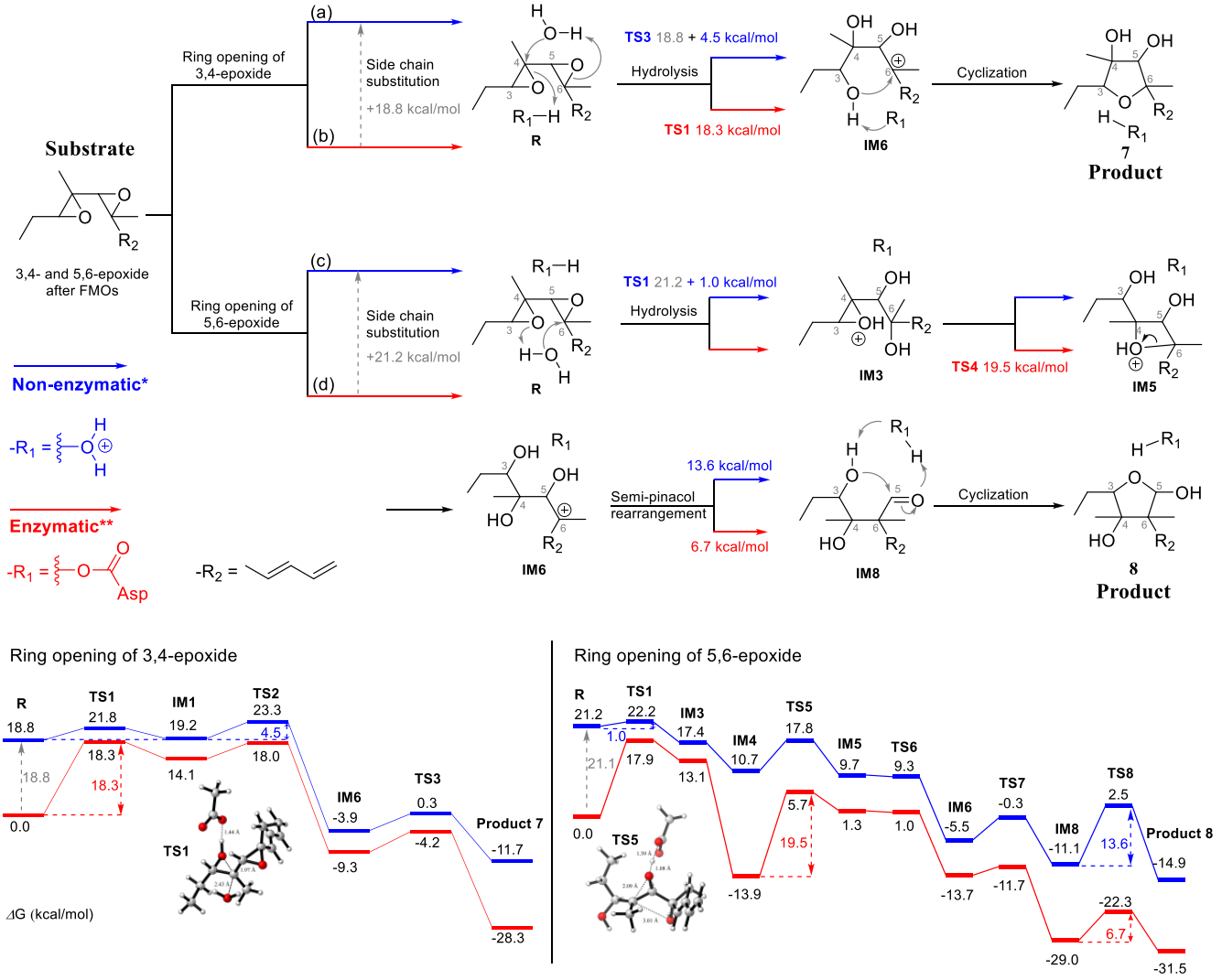

[a]All pathways start with the same epoxide substrate along with hydrolysis at 3,4-epoxide in enzymatic (route a in red) or nonenzymatic (route b in blue) reactions for **7** biosynthesis, or hydrolysis at 5,6-epoxide in enzymatic (route c in red) or nonenzymatic (route d in blue) reactions, followed by the semipinacol rearrangement for **8** biosynthesis. The energy profiles of ring-opening of 3,4-epoxide and 5,6-epoxide with the geometric structures **TS1** and **TS5** are shown above, respectively. *a hydrated proton mimics the nonenzymatic (water) environment. **an acetic acid that mimics the aspartic acid residue in the enzyme active site.

Density Functional Theory (DFT) Calculations for Asp-Aided Hydrolysis and SPR. Next, DFT chemical calculations were performed to further investigate the possible structures of transitional reactants and probe the different catalytic mechanisms between AstD/MrvD and AurD/CtvD partners to produce **8** and **7**, respectively, as well as the essentiality of the conserved Asp residue for efficient hydrolysis and SPR.

The enzymatic system was simplified by adding acetic acid to mimic the critical Asp residues in all EHs. Our computational results suggested that the different spatial locations of acidic residues in enzymes on the bis-epoxide substrates would result in distinctive ring-opening reactions at 3,4-epoxide or 5,6-epoxide for compound **7** or **8**, respectively (Figure S34). In detail, for the biosynthesis of aurovertins, if Asp-facilitated protonation for the hydrolysis at 3,4-epoxide occurs (AurD/CtvD) as proposed previously[22] (Scheme 1b, route a, and Scheme 2, route a), the propylene carbocation intermediate **IM6** forms, and the energy barrier of this rate-determining step is at least 18.3 kcal/mol (Figure S35). After deprotonation of C3−OH by Asp, nucleophilic attack of the C3 oxygen toward C6 carbocation will directly result in the cyclic product **7** (Scheme 2, route a). Biosynthesis of **1** and citreoviridin has been traditionally proposed for hydrolysis in this way (Schemes 1b, route b, and S4). However, our DFT calculations showed the other favorite ring-opening pathway catalyzed by AstD/MrvD to produce **8** (Schemes 1b, route c, and 2, route c, and Figure S36). Asp-assisted hydrolysis initially occurs at 5,6-epoxide to produce **IM3**, followed by the second ring-opening reaction at 3,4-epoxide for the intermediate **IM5**, and the subsequent intermediate **IM6** with C6 carbocation. Finally, SPR occurs at **IM6** for aldehyde and the hemiacetal **8**. In this pathway, the second ring-opening at 3,4-epoxide is the rate-determining step with an energy barrier of at least 19.5 kcal/mol.

https://doi.org/10.1021/acscatal.1c03899
ACS Catal. 2021, 11, 14702−14711

Meanwhile, a hydrated proton was used to substitute the critical Asp to mimic the nonenzymatic catalytic environment (without EHs or with Asp point mutant EHs) (Scheme 2, routes b and d). The energy in the nonenzymatic system increases to 18.8−21.2 kcal/mol in comparison to the enzymatic system, implying the instability of strong acidic conditions. After the high energy starting point, the energy barriers for the formation of **7** and **8** are 4.5 kcal/mol and 13.6 kcal/mol, respectively, indicating that the formation of **7** has superiority over **8** in the nonenzymatic catalytic environment. In addition, it was also noticed that during the SPR, the energy barrier in the nonenzymatic system (13.6 kcal/mol) is about two times higher than that in the enzymatic system (6.7 kcal/mol) (Scheme 2, routes c and d, and Figure S37), further emphasizing the importance of Asp for the SPR. These DFT calculations implied that the regio-selectivity of hydrolysis by EHs was the prerequisite for the SPR.

Overall, our data suggested that AstD/MrvD catalyze the ring-opening reactions at 5,6-epoxide (Scheme 1b, route c) for their efficient hydrolysis and subsequent SPR, which is totally different from the previous hypothesis of hydrolysis at 3,4-epoxide (Scheme 1b, route b), as adopted from the biosynthesis of aurovertins and citreoviridin (Scheme S4).

DISCUSSION

The SPR is important for asymmetric synthesis to confer the structural diversity and complexity of compounds, and SPases have been shown to have efficient and elegant catalytic activities of the SPR in high regio-/stereo-specificity during natural product biosynthesis. However, few SPases have been identified in limited enzyme families, and all discovered SPases showed catalysis of the SPR on alkaloids after oxidations (epoxidation or hydroxylation). One SPase (FtmG) catalyzes type II SPR with an allylic alcohol as the substrates[13] and two SPases (BvnE and AuaG) catalyze type IV SPR.[12,16] However, other SPases (NotB, PhqK, FqzB, CtdE, NotI/NotI′, CyaH)[8,9,11,13−15] are oxidases and catalyze epoxidation-coupled type III SPR in an R3 → C3 2,3-migration manner, to shift the substituent groups and confer the structural complexity, such as spirocycles[9] (Schemes S1−S3).

Here, two novel SPases AstD/MrvD belonging to the EH family were identified from the biosynthetic pathway of the fungal polyketide-type mycotoxin asteltoxin. They are bifunctional enzymes, working as EHs for regio-selective epoxide ring-opening on the bis-epoxide and subsequently SPases on the epoxy alcohol intermediate for structural complexity. Although these two enzymes also catalyze the type III SPR for 2,3-migration, they can recognize epoxy alcohol and catalyze the rearrangement of the polyketide backbone in C1 → C3 migration (Scheme 1).

EHs have been widely used for the synthesis of chirality-desired compounds with epoxides as native substrates.[35−39] They are involved in epoxide ring-opening in high regio-/stereo-specificity for the asymmetric biosynthesis of complex natural products with intriguing building blocks, such as enantio-pure vicinal diols, polyether, and other structural moieties.[37,40−42] There is no report of bifunctional enzymes or enzymatic cascades for these coupled epoxide hydrolysis and SPR. Thus, our work has expanded the SPase family.

We further identified critical Asp residues in these SPases as general acids for their catalysis. DFT calculations showed that the spatial location of these key Asps was essential for regio-specific hydrolysis and subsequent SPR, which might be one of the main reasons why AurD/CtvD could not execute the SPR. The introduction of this key Asp could dramatically reduce the energy barriers of both catalytic activities (Scheme 2). Thus, we introduced a modified proposed pathway for AstD-catalyzed regio-selective hydrolysis and SPR for **1** biosynthesis (Scheme 1b, route c).

Benefiting from rapidly developed *de novo* protein structure prediction based on artificial intelligence (AI), structures of four SPases were computationally obtained from Tencent AI lab (https://drug.ai.tencent.com/console/en/tfold) (Figure S38). The three-dimensional (3D) models showed α-helix-rich structures along with seven transmembrane domains, as well as a hydrophobic pocket for substrate binding in each SPase. After the molecular docking of SPases with the proposed bis-epoxide substrate **9** by Autodock (Figure S39), these four EHs showed distinctive shapes of the hydrophobic pockets, which led to the different orientations of the substrate inside. Despite the discrepancy in pockets, the carboxyl groups of the identified critical Asp in all SPases were in high proximity with the epoxide oxygen. Moreover, the critical Asp residue was apparently much closer to 5,6-epoxide than 3,4-epoxide in AstD/MrvD, but the distance discrepancy was reversed in AurD/CtvD, which was consistent with the prediction from DFT calculations for regio-selective hydrolysis.

We also showed that two conserved residues T94/S96 were required for proper hydrolysis and SPR, since MrvD^{T94P}/MrvD^{S96C} mutants conferred null production of **8** and almost identical metabolite profiles to the MrvD^{D313A} mutant after pathway reconstitution in yeast (Figure 3a). These two critical residues were found located around the binding pocket (Figure S40). Based on *de novo* protein structure prediction, the structural models of wild-type MrvD and mutants MrvD^{T94P} and MrvD^{S96C} were almost the same in the overall conformation, after superimposing these active sites (Figure S41). Therefore, we constructed systems of MrvD, MrvD^{T94P}, and MrvD^{S96C} complexed with the substrate. Three replicas of 30 ns MD simulations were performed for each system. During the dynamic simulations, the active pockets exhibited slightly different change trends for each system. Based on the structural characteristics, different binding conformations of the substrate were maintained in the most representative structure for these systems. The distributions of distances d(Asp313$_{C\gamma}$-Sub$_{O3,4}$) and d(Asp313$_{C\gamma}$-Sub$_{O5,6}$), which represented the 3,4-epoxide and 5,6-epoxide hydrolysis, respectively, revealed that T94P and S96C mutations could influence the reaction distances between D313 and the substrate. For the MrvD system, the distance d(Asp313$_{C\gamma}$-Sub$_{O3,4}$) was concentrated, while the distributions of distances d(Asp313$_{C\gamma}$-Sub$_{O3,4}$) and d-(Asp313$_{C\gamma}$-Sub$_{O5,6}$) in two mutant systems were scattered and the distances could be enlarged to 12 Å, which was unbeneficial for enzyme-catalyzed hydrolysis (Figure S41). These models were consistent with our observations that mutations of T94 and S96 led to loss-of-function in hydrolysis catalysis and subsequent SPR.

Six critical residues (G127/A201/Q314/A317/A318/M321) of MrvD for efficient SPR were also identified, and mutations of these residues significantly decreased the production of **8** (Figures S30−S32). Here, residues G127/Q314/A317/A318/M321 in MrvD were predicted to be located around the hydrophobic pocket (Figure S40). These residues are nonpolar or hydrophobic amino acids (G, A, Q, M). Two mutations Q314K and A318V in MrvD particularly reduced **8** production, suggesting subtle changes of the side-

https://doi.org/10.1021/acscatal.1c03899
ACS Catal. 2021, 11, 14702−14711

chain charge, and the steric hindrance significantly affected the SPR efficiency. In MrvD, G127 was embedded in the transmembrane domain, while the other four residues were in high proximity to the key D313 (Figure S26). We proposed that these residues formed a favorable anhydrous microenvironment to facilitate regio-specific ring-opening by D313 or protect the carbocation from attacks of water molecules or the proximal hydroxyl groups within the substrate. Therefore, mutations in these residues might reduce the regio-selectivity of hydrolysis and eventually lead to the decreased production of **8**. In the other way, mutations of these residues might result in a more facile quenching of the carbocation by the hydroxyl group for direct cyclization and therefore reduced SPR, as the energy barrier for **7** production (from direct cyclization) was 3.4 or 5.0 kcal/mol (Figure S35), lower than that for the rearrangement (6.7 kcal/mol) (Scheme 2).

Overall, this work identified two new SPases from the fungal EH family and explored possible mechanisms for regio-specific hydrolysis and efficient SPR. These EH family SPases adopted distinctive orientation for epoxide collapse and a more favorable enzymatic pocket for the SPR compared with the canonical EHs without SPR catalytic activity. This work will be helpful for understanding and further engineering these powerful biocatalysts for asymmetric biosynthesis of complex compounds.

CONCLUSIONS

SPases are intriguing biocatalysts for structural diversity and complexity of natural products, but only a few of them have been identified and characterized. Here, based on the biosynthesis of a fungal mycotoxin asteltoxin, two new bifunctional SPases AstD/MrvD were identified, which possessed both EH and SPase catalytic activities for the cascade reactions of regio-selective hydrolysis on the bis-epoxide and SPR on the epoxide alcohol. They catalyze C1 → C3 migration on the polyketide backbone as type III SPR. A conserved Asp residue was proposed to be essential for both catalysis, and other critical residues form a microenvironment to facilitate efficient epoxide hydrolysis and proper SPR. Our discovery expanded the SPR biocatalyst family and provided a new understanding of the catalytic mechanisms of these novel bifunctional SPases.

ASSOCIATED CONTENT

Supporting Information

The Supporting Information is available free of charge at https://pubs.acs.org/doi/10.1021/acscatal.1c03899.

Methods describing additional experimental details, materials, and methods, including gene cloning, plasmid construction, extraction of fungal metabolic profiles, HPLC and LC-MS analysis, isolation and characterization of compounds, and computational details, as well as supplementary experimental data (PDF)

AUTHOR INFORMATION

Corresponding Authors

Zha-Jun Zhan − *College of Pharmaceutical Science, Zhejiang University of Technology, Hangzhou 310014, China;* orcid.org/0000-0001-7865-5435; Email: zjnpr@zjut.edu.cn

Ting Shi − *State Key Laboratory of Microbial Metabolism, Joint International Research Laboratory of Metabolic and Developmental Sciences, School of Life Sciences and Biotechnology, Shanghai Jiao Tong University, Shanghai 200240, China;* orcid.org/0000-0003-3921-4412; Email: tshi@sjtu.edu.cn

Xu-Ming Mao − *Research Center for Clinical Pharmacy, The First Affiliated Hospital & Institute of Pharmaceutical Biotechnology, School of Medicine, Zhejiang University, Hangzhou 310058, China; State Key Laboratory of Bioactive Substance and Function of Natural Medicines, Institute of Materia Medica, Chinese Academy of Medical Sciences and Peking Union Medical College, Beijing 100050, China; Zhejiang Provincial Key Laboratory for Microbial Biochemistry and Metabolic Engineering, Zhejiang University, Hangzhou 310058, China;* orcid.org/0000-0003-0669-7630; Email: xmmao@zju.edu.cn

Authors

Fei Cao − *Research Center for Clinical Pharmacy, The First Affiliated Hospital & Institute of Pharmaceutical Biotechnology, School of Medicine, Zhejiang University, Hangzhou 310058, China; Zhejiang Provincial Key Laboratory for Microbial Biochemistry and Metabolic Engineering, Zhejiang University, Hangzhou 310058, China*

Wen-Tao Tao − *State Key Laboratory of Microbial Metabolism, Joint International Research Laboratory of Metabolic and Developmental Sciences, School of Life Sciences and Biotechnology, Shanghai Jiao Tong University, Shanghai 200240, China; Clinical Research Center, Shanghai Chest Hospital, Shanghai Jiao Tong University, Shanghai 200030, China*

Qian Yu − *State Key Laboratory of Microbial Metabolism, Joint International Research Laboratory of Metabolic and Developmental Sciences, School of Life Sciences and Biotechnology, Shanghai Jiao Tong University, Shanghai 200240, China*

Chu-Xuan Xu − *Research Center for Clinical Pharmacy, The First Affiliated Hospital & Institute of Pharmaceutical Biotechnology, School of Medicine, Zhejiang University, Hangzhou 310058, China; Zhejiang Provincial Key Laboratory for Microbial Biochemistry and Metabolic Engineering, Zhejiang University, Hangzhou 310058, China*

Jin-Tao Cheng − *Research Center for Clinical Pharmacy, The First Affiliated Hospital & Institute of Pharmaceutical Biotechnology, School of Medicine, Zhejiang University, Hangzhou 310058, China; Zhejiang Provincial Key Laboratory for Microbial Biochemistry and Metabolic Engineering, Zhejiang University, Hangzhou 310058, China*

Ruo-Xi Liu − *College of Pharmaceutical Science, Zhejiang University of Technology, Hangzhou 310014, China*

Qing-Wei Zhao − *Research Center for Clinical Pharmacy, The First Affiliated Hospital & Institute of Pharmaceutical Biotechnology, School of Medicine, Zhejiang University, Hangzhou 310058, China; Zhejiang Provincial Key Laboratory for Microbial Biochemistry and Metabolic Engineering, Zhejiang University, Hangzhou 310058, China*

Xin-Hang Jiang − *Equipment and Technology Service Platform, College of Life Science, Zhejiang University, Hangzhou 310058, China*

Yu Liu − *Equipment and Technology Service Platform, College of Life Science, Zhejiang University, Hangzhou 310058, China*

Yong-Quan Li − *Research Center for Clinical Pharmacy, The First Affiliated Hospital & Institute of Pharmaceutical*

Biotechnology, School of Medicine, Zhejiang University, Hangzhou 310058, China; Zhejiang Provincial Key Laboratory for Microbial Biochemistry and Metabolic Engineering, Zhejiang University, Hangzhou 310058, China; orcid.org/0000-0001-6013-4068

Complete contact information is available at: https://pubs.acs.org/10.1021/acscatal.1c03899

Author Contributions

F.C., Z-J.Z., T.S., and X-M.M. designed the experiments; F.C., W.-T.T., Q.Y., C.-X.X, J.-T.C., R.-X.L., X.-H.J., and Y.L. conducted the experiments; F.C., W.-T.T., Q.-W.Z., Y.-Q.L., Z.-J.Z., T.S., and X.-M.M. analyzed the data; F.C., W.-T.T., Z.-J.Z., T.S., and X.-M.M. prepared the manuscript, and all authors read and approved the final manuscript for publication.

Funding

This work was financially supported by the National Natural Science Foundation of China (31520103901, 31770071, 32070039, 32070041, 81872777) and the National Key R&D Program of China (2019YFA0905400).

Notes

The authors declare no competing financial interest.

■ ACKNOWLEDGMENTS

The authors thank Prof. Weiguo Fang in College of Life Sciences, Zhejiang University, for his kind gifts of two fungal strains *M. anisopliae* ARSEF 549 and *M. robertsii* ARSEF 2575. We will also highly appreciate Prof. Yi Tang at the University of California, Los Angeles (UCLA), and Prof. Yi Zou in College of Pharmaceutical Sciences and Chinese Medicine, Southwest University, China, for their critical reading and helpful comments to improve this manuscript.

■ REFERENCES

(1) Nagaraju, K.; Ni, D.; Ma, D. Total synthesis of kopsinitarine E. *Angew. Chem., Int. Ed.* **2020**, *59*, 22039−22042.
(2) Wu, X.; Chen, C.; Guo, Z.; North, M.; Whitwood, A. Metal-and halide-free catalyst for the synthesis of cyclic carbonates from epoxides and carbon dioxide. *ACS Catal.* **2019**, *9*, 1895−1906.
(3) Wang, B.; Tu, Y. Q. Stereoselective construction of quaternary carbon stereocenters via a semipinacol rearrangement strategy. *Acc. Chem. Res.* **2011**, *44*, 1207−1222.
(4) Song, Z. L.; Fan, C. A.; Tu, Y. Q. Semipinacol rearrangement in natural product synthesis. *Chem. Rev.* **2011**, *111*, 7523−7556.
(5) Kita, Y.; Matsuda, S.; Inoguchi, R.; Ganesh, J. K.; Fujioka, H. Lewis acid-promoted rearrangement of 2,3-epoxy alcohol derivatives: stereochemical control and selective formation of two types of chiral quaternary carbon centers from the single carbon skeleton. *J. Org. Chem.* **2006**, *71*, 5191−5197.
(6) Tanveer, K.; Kim, S. J.; Taylor, M. S. Borinic acid/halide co-catalyzed semipinacol rearrangements of 2,3-epoxy alcohols. *Org. Lett.* **2018**, *20*, 5327−5331.
(7) Matsubara, S.; Yamamoto, H.; Oshima, K. Stereoselective pinacol-type rearrangement of 2,3-epoxy alcohols with retention of configuration mediated by bis(iodozincio)methane. *Angew. Chem., Int. Ed.* **2002**, *41*, 2837−2840.
(8) Fraley, A. E.; Tran, H. T.; Kelly, S. P.; Newmister, S. A.; Tripathi, A.; Kato, H.; Tsukamoto, S.; Du, L.; Li, S.; Williams, R. M.; Sherman, D. H. Flavin-dependent monooxygenases NotI and NotI' mediate spiro-oxindole formation in biosynthesis of the notoamides. *ChemBioChem* **2020**, *21*, 2449−2454.
(9) Fraley, A. E.; Caddell Haatveit, K.; Ye, Y.; Kelly, S. P.; Newmister, S. A.; Yu, F.; Williams, R. M.; Smith, J. L.; Houk, K. N.; Sherman, D. H. Molecular basis for spirocycle formation in the paraherquamide biosynthetic pathway. *J. Am. Chem. Soc.* **2020**, *142*, 2244−2252.
(10) Matsushita, T.; Kishimoto, S.; Hara, K.; Hashimoto, H.; Watanabe, K. structural and functional analyses of a spiro-carbon-forming, highly promiscuous epoxidase from fungal natural product biosynthesis. *Biochemistry* **2020**, *59*, 4787−4792.
(11) Li, S.; Finefield, J. M.; Sunderhaus, J. D.; McAfoos, T. J.; Williams, R. M.; Sherman, D. H. Biochemical characterization of NotB as an FAD-dependent oxidase in the biosynthesis of notoamide indole alkaloids. *J. Am. Chem. Soc.* **2012**, *134*, 788−791.
(12) Katsuyama, Y.; Harmrolfs, K.; Pistorius, D.; Li, Y.; Müller, R. A Semipinacol Rearrangement directed by an enzymatic system featuring dual-function FAD-dependent monooxygenase. *Angew. Chem., Int. Ed.* **2012**, *51*, 9437−9440.
(13) Tsunematsu, Y.; Ishikawa, N.; Wakana, D.; Goda, Y.; Noguchi, H.; Moriya, H.; Hotta, K.; Watanabe, K. Distinct mechanisms for spiro-carbon formation reveal biosynthetic pathway crosstalk. *Nat. Chem. Biol.* **2013**, *9*, 818−825.
(14) Liu, Z.; Zhao, F.; Zhao, B.; Yang, J.; Ferrara, J.; Sankaran, B.; Venkataram Prasad, B. V.; Kundu, B. B.; Phillips, G. N., Jr.; Gao, Y.; Hu, L.; Zhu, T.; Gao, X. Structural basis of the stereoselective formation of the spirooxindole ring in the biosynthesis of citrinadins. *Nat. Commun.* **2021**, *12*, No. 4158.
(15) Zhu, Y.; Zhang, Q.; Fang, C.; Zhang, Y.; Ma, L.; Liu, Z.; Zhai, S.; Peng, J.; Zhang, L.; Zhu, W.; Zhang, C. Refactoring the concise biosynthetic pathway of cyanogramide unveils spirooxindole formation catalyzed by a P450 enzyme. *Angew. Chem., Int. Ed.* **2020**, *59*, 14065−14069.
(16) Ye, Y.; Du, L.; Zhang, X.; Newmister, S. A.; McCauley, M.; Alegre-Requena, J. V.; Zhang, W.; Mu, S.; Minami, A.; Fraley, A. E.; Adrover-Castellano, M. L.; Carney, N. A.; Shende, V. V.; Qi, F.; Oikawa, H.; Kato, H.; Tsukamoto, S.; Paton, R. S.; Williams, R. M.; Sherman, D. H.; Li, S. Fungal-derived brevianamide assembly by a stereoselective semipinacolase. *Nat. Catal.* **2020**, *3*, 497−506.
(17) Vleggaar, R. Biosynthetic studies on some polyene mycotoxins. *Pure Appl. Chem.* **1986**, *58*, 239−256.
(18) Steyn, P. S.; Vleggaar, R. Biosynthesis of asteltoxin by cultures of *Emericella variecolor* - the role of propionate in the biosynthesis and evidence for a 1,2-bond migration in the formation of the bistetrahydrofuran moiety. *J. Chem. Soc., Chem. Commun.* **1984**, 977−979.
(19) Kruger, G. J.; Steyn, P. S.; Vleggaar, R.; Rabie, C. J. X-Ray crystal structure of asteltoxin, a novel mycotoxin from *Aspergillus stellatus* curzi. *J. Chem. Soc., Chem. Commun.* **1979**, 441−442.
(20) Kiyoshi, K.; Fukushima, H.; Nozawa, Y. Inhibition of mitochondrial respiration by asteltoxin, a respiratory toxin from *Emericella variecolor*. *Toxicol. Lett.* **1985**, *28*, 73−77.
(21) Eom, K. D.; Raman, J. V.; Kim, H.; Cha, J. K. Total synthesis of (+)-asteltoxin. *J. Am. Chem. Soc.* **2003**, *125*, 5415−5421.
(22) Mao, X. M.; Zhan, Z. J.; Grayson, M. N.; Tang, M. C.; Xu, W.; Li, Y. Q.; Yin, W. B.; Lin, H. C.; Chooi, Y. H.; Houk, K. N.; Tang, Y. Efficient biosynthesis of fungal polyketides containing the dioxabicyclo-octane ring system. *J. Am. Chem. Soc.* **2015**, *137*, 11904−11907.
(23) Van Raaij, M. J.; Abrahams, J.; Leslie, A.; Walker, J. E. The structure of bovine F1-ATPase complexed with the antibiotic inhibitor aurovertin B. *Proc. Natl. Acad. Sci. U.S.A.* **1996**, *93*, 6913−6917.
(24) Lin, T. S.; Chiang, Y. M.; Wang, C. C. Biosynthetic pathway of the reduced polyketide product citreoviridin in *Aspergillus terreus var. aureus* revealed by heterologous expression in *Aspergillus nidulans*. *Org. Lett.* **2016**, *18*, 1366−1369.
(25) Linnett, P. E.; Mitchell, A.; Osselton, M.; Mulheirn, L.; Beechey, R. Citreoviridin, a specific inhibitor of the mitochondiral adenosine triphosphatase. *Biochem. J.* **1978**, *170*, 503−510.
(26) Mount, D. W. Using the basic local alignment search tool (BLAST). *Cold Spring Harbor Protoc.* **2007**, *2007*, top17.
(27) Ma, S. M.; Li, J. W. H.; Choi, J. W.; Zhou, H.; Lee, K. K. M.; Moorthie, V. A.; Xie, X. K.; Kealey, J. T.; Da Silva, N. A.; Vederas, J.

C.; Tang, Y. Complete reconstitution of a highly reducing iterative polyketide synthase. *Science* **2009**, *326*, 589−592.
(28) Fujii, I.; Hashimoto, M.; Konishi, K.; Unezawa, A.; Sakuraba, H.; Suzuki, K.; Tsushima, H.; Iwasaki, M.; Yoshida, S.; Kudo, A.; et al. Shimalactone biosynthesis involves spontaneous double bicyclo-ring formation with 8π-6π electrocyclization. *Angew. Chem., Int. Ed.* **2020**, *59*, 8464−8470.
(29) Kahlert, L.; Bassiony, E. F.; Cox, R. J.; Skellam, E. Diels−Alder reactions during the biosynthesis of sorbicillinoids. *Angew. Chem., Int. Ed.* **2020**, *59*, 5816−5822.
(30) Chen, Y. R.; Naresh, A.; Liang, S. Y.; Lin, C. H.; Chein, R. J.; Lin, H. C. Discovery of a dual function cytochrome P450 that catalyzes enyne formation in cyclohexanoid terpenoid biosynthesis. *Angew. Chem., Int. Ed.* **2020**, *59*, 13537−13541.
(31) Lai, C. Y.; Lo, I. W.; Hewage, R. T.; Chen, Y. C.; Chen, C. T.; Lee, C. F.; Lin, S.; Tang, M. C.; Lin, H. C. Biosynthesis of complex indole alkaloids: elucidation of the concise pathway of okaramines. *Angew. Chem., Int. Ed.* **2017**, *56*, 9478−9482.
(32) Hopmann, K. H.; Hallberg, B. M.; Himo, F. Catalytic mechanism of limonene epoxide hydrolase, a theoretical study. *J. Am. Chem. Soc.* **2005**, *127*, 14339−14347.
(33) Nardini, M.; Rink, R.; Janssen, D. B.; Dijkstra, B. W. Structure and mechanism of the epoxide hydrolase from *Agrobacterium radiobacter* AD1. *J. Mol. Catal. B: Enzym.* **2001**, *11*, 1035−1042.
(34) Zou, Y.; Garcia-Borras, M.; Tang, M. C.; Hirayama, Y.; Li, D. H.; Li, L.; Watanabe, K.; Houk, K. N.; Tang, Y. Enzyme-catalyzed cationic epoxide rearrangements in quinolone alkaloid biosynthesis. *Nat. Chem. Biol.* **2017**, *13*, 325−332.
(35) Chen, Y.; Chen, C.; Wu, X. Dicarbonyl reduction by single enzyme for the preparation of chiral diols. *Chem. Soc. Rev.* **2012**, *41*, 1742−1753.
(36) Sun, C. P.; Zhang, X. Y.; Morisseau, C.; Hwang, S. H.; Zhang, Z. J.; Hammock, B. D.; Ma, X. C. Discovery of soluble epoxide hydrolase inhibitors from chemical synthesis and natural products. *J. Med. Chem.* **2021**, *64*, 184−215.
(37) Saini, P.; Sareen, D. An overview on the enhancement of enantioselectivity and stability of microbial epoxide hydrolases. *Mol. Biotechnol.* **2017**, *59*, 98−116.
(38) Riera, A.; Moreno, M. Synthetic applications of chiral unsaturated epoxy alcohols prepared by sharpless asymmetric epoxidation. *Molecules* **2010**, *15*, 1041−1073.
(39) Fu, J.; Gu, Y.; Yuan, H.; Luo, T.; Liu, S.; Lan, Y.; Gong, J.; Yang, Z. Towards a general diastereoselective route to oxabicyclo[3.2.1]octanes via a gold-catalysed cascade reaction. *Nat. Commun.* **2015**, *6*, No. 8617.
(40) Zheng, Q.; Wang, S.; Duan, P.; Liao, R.; Chen, D.; Liu, W. An alpha/beta-hydrolase fold protein in the biosynthesis of thiostrepton exhibits a dual activity for endopeptidyl hydrolysis and epoxide ring opening/macrocyclization. *Proc. Natl. Acad. Sci. U.S.A.* **2016**, *113*, 14318−14323.
(41) Hotta, K.; Chen, X.; Paton, R. S.; Minami, A.; Li, H.; Swaminathan, K.; Mathews, I. I.; Watanabe, K.; Oikawa, H.; Houk, K. N.; Kim, C. Y. Enzymatic catalysis of anti-Baldwin ring closure in polyether biosynthesis. *Nature* **2012**, *483*, 355−358.
(42) Wang, L.; Parnell, A.; Williams, C.; Bakar, N. A.; Challand, M. R.; van der Kamp, M. W.; Simpson, T. J.; Race, P. R.; Crump, M. P.; Willis, C. L. A Rieske oxygenase/epoxide hydrolase-catalysed reaction cascade creates oxygen heterocycles in mupirocin biosynthesis. *Nat. Catal.* **2018**, *1*, 968−976.

https://doi.org/10.1021/acscatal.1c03899
ACS Catal. 2021, 11, 14702−14711